

# **Digital Wideband Linear-FM Chirp Waveform Generator**

D.G. Kocher

29 December 2010

---

**Lincoln Laboratory**  
MASSACHUSETTS INSTITUTE OF TECHNOLOGY  
*LEXINGTON, MASSACHUSETTS*



---

Prepared for the Rapid Reaction Technology Office/Defense Research & Engineering  
under Air Force Contract FA8721-05-C-0002.

Approved for public release; distribution is unlimited.

**20110110647**



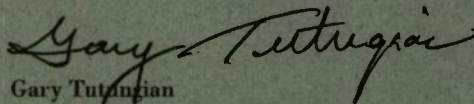
This report is based on studies performed at Lincoln Laboratory, a center for research operated by Massachusetts Institute of Technology. This work was sponsored by the Rapid Reaction Technology Office/Defense Research & Engineering, RRTO/DDR&E, under Contract FA8721-05-C-0002.

This report may be reproduced to satisfy needs of U.S. Government agencies.

The 66ABW Public Affairs Office has reviewed this report, and it is releasable to the National Technical Information Service, where it will be available to the general public, including foreign nationals.

This technical report has been reviewed and is approved for publication.

FOR THE COMMANDER



Gary Tutunjian  
Administrative Contracting Officer  
Plans and Programs Directorate  
Contracted Support Management

Non-Lincoln Recipients

PLEASE DO NOT RETURN

Permission has been given to destroy this document when it is no longer needed.

Massachusetts Institute of Technology  
Lincoln Laboratory

Digital Wideband Linear-FM Chirp Waveform Generator

*D.G. Kocher*  
*Group 106*

Technical Report 1157

29 December 2010

Approved for public release; distribution is unlimited.

Lexington

Massachusetts

This page intentionally left blank.

## ABSTRACT

The design and performance of a digital linear-FM chirp waveform microwave generator having a maximum bandwidth capability of 16 GHz and minimum chirp duration of 102.4 ns are described along with techniques developed for the compensation of hardware errors. Emphasis is on optimization and characterization of chirp quality while operating with large bandwidths and chirp durations less than a microsecond.

This page intentionally left blank.

## ACKNOWLEDGMENTS

The steadfast support of Drs. Richard M. Heinrichs and Sumanth Kaushik in arranging for the time and resources for the work reported here is gratefully acknowledged. Technical discussions with Dr. Kevin W. Holman have been very helpful.

This page intentionally left blank.



## TABLE OF CONTENTS

Abstract	iii
Acknowledgments	v
List of Illustrations	ix
1. INTRODUCTION	1
2. DESIGN	3
2.1 Design Considerations	3
2.2 Block Diagram	4
2.3 Frequency-Doubler Power Response	6
3. CALIBRATION	9
3.1 Static Calibration	9
3.2 Chirp Waveform Computation	10
3.3 Dynamic Calibration	11
4. CARRIER LEAKAGE SUPPRESSION	15
4.1 Exposing the Carrier Leakage	15
4.2 Carrier Null Servo	15
5. PERFORMANCE	17
5.1 SSBM Output Spectra	17
5.2 Chirp Stop-Start Transients	19
5.3 Time-Sidelobe Levels	21
5.4 Chirp Spectra at the WFG Output	22
6. SUMMARY	27
References	29

This page intentionally left blank.

## LIST OF ILLUSTRATIONS

Figure No.		Page
1	High-level block diagram of the waveform generator system.	4
2	Photograph of the WFG.	5
3	Power transfer curves for the four frequency doublers, identified by their input-output frequencies in GHz.	7
4	CW waveform drive amplitude A required for uniform WFG output levels.	10
5	Differential amplitude and phase required to minimize the unwanted sideband during CW waveform generation.	10
6	Residuals after the best linear fit to correlator null frequency values over the frequency range 2–18 GHz.	13
7	Predicted phase error of a 2–18 GHz, 512 ns chirp due to correlator errors.	13
8	Superimposed SSBM CW output spectra, using static correction only. The modulating frequencies are 188, 292, 396, and 495 MHz.	17
9	SSBM output spectrum of a +350 to +450 MHz, 512 ns period repetitive chirp train.	18
10	SSBM output spectrum of a +350 to +450 MHz, 102.4 ns period repetitive chirp train.	19
11	SSBM output spectrum of a +250 to +450 MHz, 102.4 ns period repetitive chirp train.	19
12	Stop (top trace) and start (lower trace) WFG output transients.	19
13	AWG I & Q outputs for a +500 MHz to –500 MHz CW waveform transition, measured with a 4 GSa/s, 1 GHz BW digital storage oscilloscope, and resampled at 2.5× for plotting.	20
14	Measured chirp amplitude and phase error of a 15.625 GHz, 640 ns dual chirp waveform after dynamic calibration.	21
15	Filtered and unfiltered correlator spectra of a 15.625 GHz, 640 ns dual chirp waveform after dynamic calibration.	21

<b>Figure No.</b>		<b>Page</b>
16	Correlator spectrum of a 12.5 GHz, 128 ns dual chirp after dynamic calibration.	22
17	Spurious frequencies in the WFG output, while generating narrow band (0.16 GHz), 512 ns chirps centered at 17.92 GHz.	23
18	Down-converter spurs for 0.8 GHz, 512 ns dual up-chirps placed across the 2–18 GHz spectrum. The ordinate of the top trace only is dBm/10 kHz BW, and the remaining spectra have been displaced vertically for clarity.	24
19	WFG output spectra of 12.5 GHz chirps for three different chirp durations.	25

## 1. INTRODUCTION

The linear-FM (LFM) chirp waveform is employed frequently in radar and ladar systems as a form of pulse compression, mitigating peak power limitations of transmitters [1]. The LFM chirp waveform can be generated with a voltage-controlled oscillator (VCO) [2, 3], or more conveniently with a digital waveform generator [4–6], the choice depending on the application, bandwidth, chirp period and, if necessary, the ease of phase-locking the waveform to a reference. Frequency doublers are employed often to increase the bandwidth of the waveform, especially in the case of digital waveform generation. Phase and amplitude errors in both the waveform generator (WFG) and in other components in the electronic signal path are undesirable and methods to measure and correct these errors are described in the literature [2], [7], [8].

This report describes the design and performance of a digital LFM chirp waveform generator provided for an application requiring repetitive, contiguous, 12.5 GHz bandwidth, 512 ns duration chirps. The generator is capable of a maximum bandwidth (BW) of 16 GHz, a minimum chirp duration of 102.4 ns, and it has a baseband clock rate of 1.25 GHz. It uses a single-sideband modulator (SSBM) to convert a base-band quadrature-pair chirp signal into an RF signal, followed by a four-stage frequency-doubler chain to increase the bandwidth sixteen times. The doubler chain output is down-converted to a center frequency of 10 GHz as required for the intended application. The application and the hardware implementation necessitated the use of special techniques to compensate for hardware imperfections. One of these is a CW or “static” calibration, determined by CW tone calibrations across the spectrum, which normalizes the amplitude through the system and simultaneously reduces the unwanted image sideband amplitude in the SSBM output. Another is a “dynamic” calibration, correcting for the effects of (time-delayed) signal reflections and phase nonlinearities in the hardware. The dynamic correction is made by optimizing the waveform quality while generating a specific LFM chirp output waveform. In addition to these compensation techniques, a technique has been devised to minimize automatically the SSBM carrier leakage during operation. Results obtained with these techniques are described for several LFM chirp waveforms.



This page intentionally left blank.

## 2. DESIGN

### 2.1 DESIGN CONSIDERATIONS

The heart of the digital waveform generator is a two-channel base-band arbitrary waveform generator (AWG) used to modulate an RF carrier at some chosen frequency. The number of subsequent frequency (and hence bandwidth) multiplications needed and the spurious signal (spur) level required to meet the system specifications influence the choice of AWG clock rate, amplitude resolution and spur level. While the base-band output of an AWG can be translated up to an RF carrier frequency with either a conventional double-sideband mixer or with a single-sideband modulator, the SSBM can provide twice the AWG bandwidth at its output, potentially eliminating the need for a subsequent frequency doubler stage, at the expense of requiring two AWG channel outputs for modulation inputs. Conversely, the conventional mixer technique provides only the output bandwidth of the AWG and some of that bandwidth may have to be sacrificed in order to reject carrier leakage and the unwanted sideband by filtering, if these levels are troublesome. Carrier leakage and image-sideband levels also can be a problem when using the single-sideband mixer technique, but methods are described here to reduce these to acceptable levels for most applications. The overall system configuration is chosen by evaluating straw designs employing available AWG's, single- or double-sideband modulators, different numbers of frequency doublers, practical bandpass filters for the frequency doubler stages, and in this case, available microwave frequency bands, all while paying attention to the spurious frequency levels present in the output.

The performance goals adopted for the design were at least 12.5 GHz LFM chirp bandwidth, chirp duration of 512 ns, with a time-sidelobe level of  $-40$  dBc. The application requires excellent chirp amplitude flatness and phase accuracy. The AWG chosen provides two channels with 15-bit resolution, at a clock rate of 1.25 GHz, with an output bandwidth of 500 MHz, with a spurious signal level of  $-65$  dBc. By using a single-sideband modulator and programming the AWG to produce quadrature SSBM modulating signals, a total of 1 GHz bandwidth is available from the SSBM (i.e., carrier frequency  $\pm 500$  MHz). Since each frequency doubler stage needed subsequently will increase the spur level by 6 dB, a maximum of four doublings is permitted before the output spur level exceeds  $-40$  dBc. Using four frequency-doubler stages after the SSBM increases the available bandwidth to 16 GHz.

Successful implementation of the SSBM technique requires the carrier leakage and the image-sideband levels also be reduced to the  $-65$  dBc level. Carrier leakage and image-sideband level variations are reduced by regulating the temperature of the SSBM. A closed-loop servo is used to automatically minimize the carrier leakage. The image-sideband level is reduced by performing CW tone calibrations at frequent intervals across the SSBM output spectrum and noting the differential amplitude and phase adjustments that must be applied to the quadrature modulation signals to null the image sideband. These adjustments are used to create a correction table across the frequency spectrum. Later, during chirp waveform computation the desired chirp signal is represented as a complex function and transformed to

the frequency domain, where the appropriate amplitude and phase corrections to minimize the image-sideband level are applied at each frequency. The corrected signal then is transformed back to the time domain to obtain the corrected AWG drive files. This correction is referred to here as the “static,” or CW, calibration technique, as it is obtained with static (CW) frequency measurements.

A subsequent dynamic correction also is necessary because of phase nonlinearities and signal reflections that vary across the frequency spectrum and with the chirp duration. The dynamic correction is determined by measuring the phase and amplitude errors in the LFM chirp output signal, and additionally modifying the chirp signal phase and amplitude during waveform computation to minimize these errors during an iterative minimization process. A different dynamic calibration is required for every chirp waveform bandwidth and duration. Waveform computation and WFG control are performed with MATLAB® software [9]. These calibration techniques are described in more detail in following sections.

## 2.2 BLOCK DIAGRAM

Figure 1 is a block diagram of the waveform generator system. The SSBM is mounted on a temperature-controlled heat sink directly in front of the AWG, so the in-phase (I) and quadrature (Q) modulating drive connections from the AWG can be shortened to 2.5 inches length to reduce the time-delay of any signal reflections. In series with the I and Q drives to the SSBM are low-pass filters combined with bias tees. The low-pass filters ensure that the clock frequency and its harmonics don't contribute significant spurs in the output spectrum of the SSBM. The bias tees are simply 3.5 k $\Omega$  resistors connected to the I and Q signal lines to permit the addition of small analog DC bias offsets to the quadrature drives to null the I and Q components of the SSMB carrier leakage. The SSBM LO frequency used is 4.2 GHz, chosen to place the 16 GHz output bandwidth of the four-stage frequency-doubler chain at the upper end of the 50–75 GHz microwave V-band. Each frequency-doubler stage typically consists of

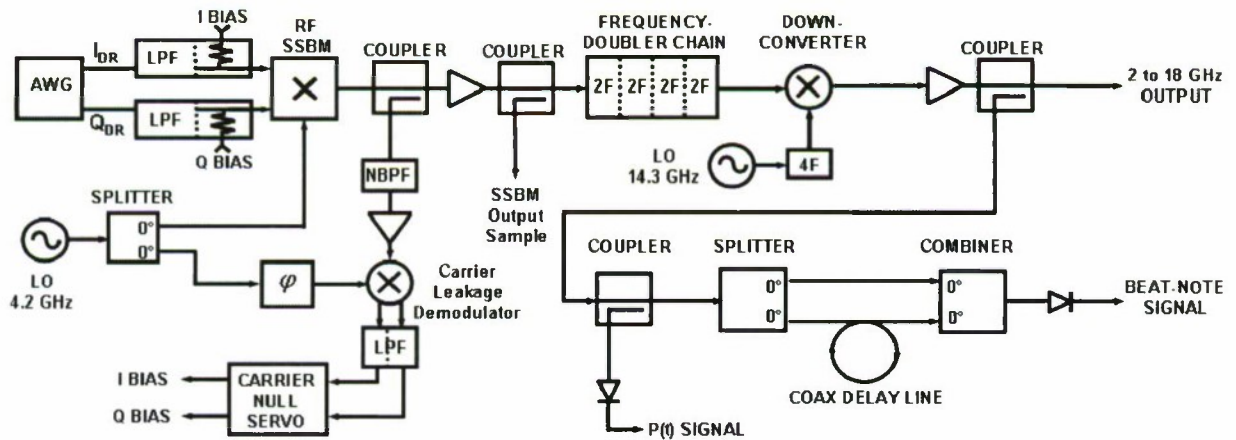
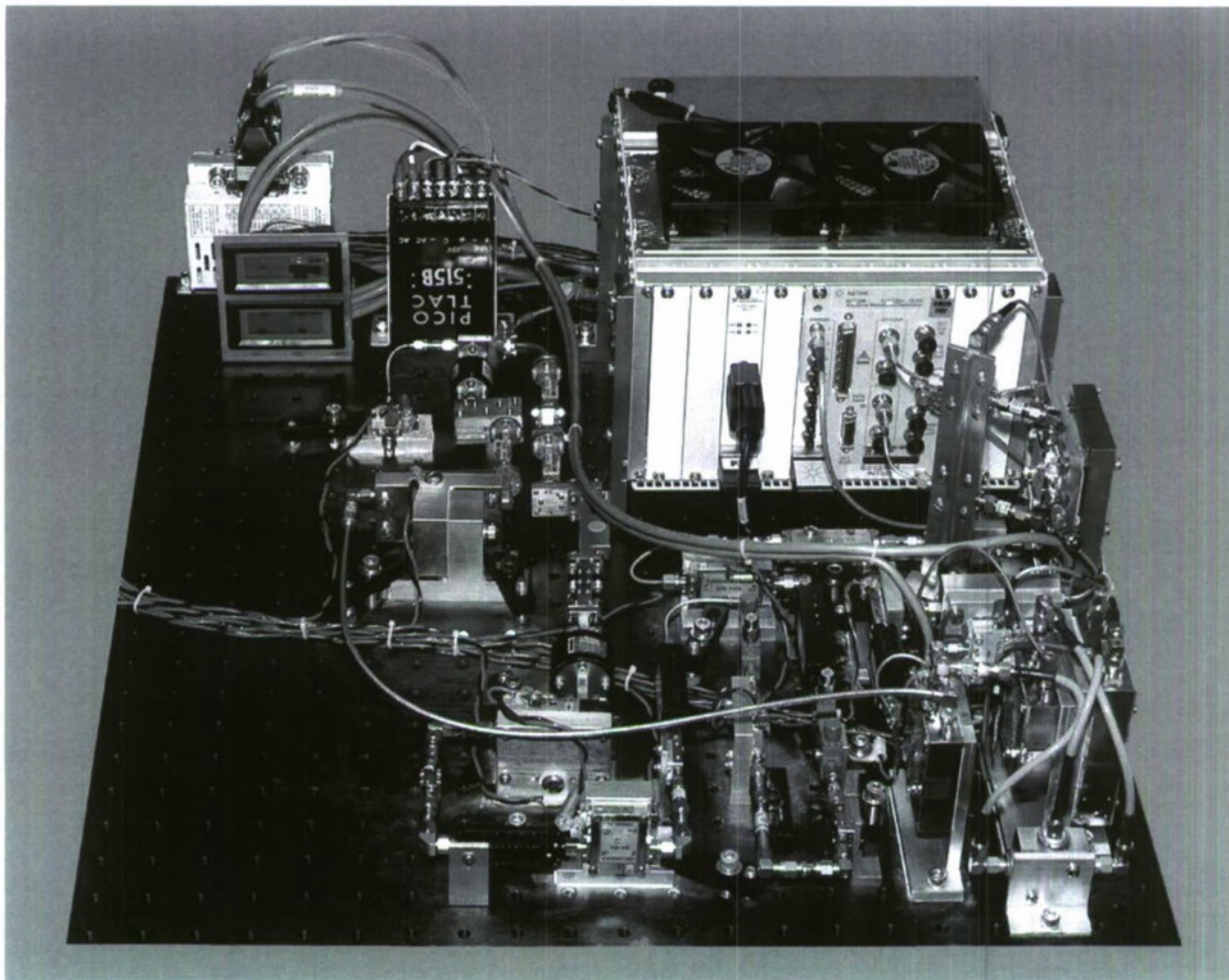


Figure 1. High-level block diagram of the waveform generator system.



an amplifier, a band-pass filter to reduce the fundamental and third and higher harmonics, a passive diode frequency doubler, and isolators as needed. The final doubler output, centered at 67.2 GHz, is down-converted to 10 GHz center frequency and low-pass filtered (filter not shown) for the present 12.5 GHz bandwidth application. An amplifier brings the output level to the required level for the application.

A carrier null servo is shown in the lower-left portion of Figure 1. A narrow band-pass filter (NBPF) tuned to the SSBM LO frequency feeds an I-Q demodulator for measuring the quadrature components of the carrier leakage. (A technique for moving the repetitive-chirp spectral line away from the LO frequency to expose carrier leakage is described below.) A two-channel servo feeds the integral of the demodulator output signals back to the bias tees to automatically null the carrier leakage. Both the SSBM and the carrier-leakage demodulator are temperature controlled.



*Figure 2. Photograph of the WFG.*

Shown in the lower-right portion of Figure 1 is a delay-line correlator used for the dynamic calibration. A coupler provides a tap to measure the output chirp power level, and the delay-line combiner and detector provides a baseband quasi-CW tone or beat note resulting from the square-law detection of the chirp signal summed with a delayed version of itself. The power signal  $P(t)$  and the beat-note signal are used during the dynamic calibration described below to correct the amplitude and phase of the chirp output.

The WFG is shown in Figure 2. Although it was implemented with connectorized RF components, all the techniques described here could be used in a miniaturized, integrated hardware implementation. Downstream of the SSBM, the heat-producing components were mounted on a 21 × 24-inch aluminum plate, which provides adequate temperature stability for these components in the laboratory environment in which the WFG has been used. The hole-grid spacing in the mounting plate is one inch square. The temperature controllers are at the left rear. The carrier-null servo, delay-line correlator and power supplies are not shown.

### 2.3 FREQUENCY-DOUBLER POWER RESPONSE

Frequency doublers typically are full-wave rectifier devices that function most efficiently at a specific power level, determined by the design and the characteristics of the semiconductor diodes used, and the power transfer function is very nonlinear. Figure 3 shows the output power at frequency  $2F$  versus the input power at frequency  $F$  for each of the four frequency doublers used in the WFG, as well a computed composite transfer curve for the four doublers in series. The drive for each doubler was chosen to be in the center of its “linear” range, usually about +13 dBm. Since in the present application it is desired to be able to correct for spectral amplitude variations in devices subsequent to the WFG, the doubler drive must be amplitude modulated during the chirp in order to hold the final output level constant. (If this were not the case, saturating amplifiers could be used in the individual doubler stages so each doubler could be driven at its optimum operating point.) Figure 3 shows that only a very limited useful “linear” amplitude leveling range is available from the doubler train, making careful adjustment of the drive levels very important. The flatter the frequency response of all the components, the more overall useable amplitude range is available.



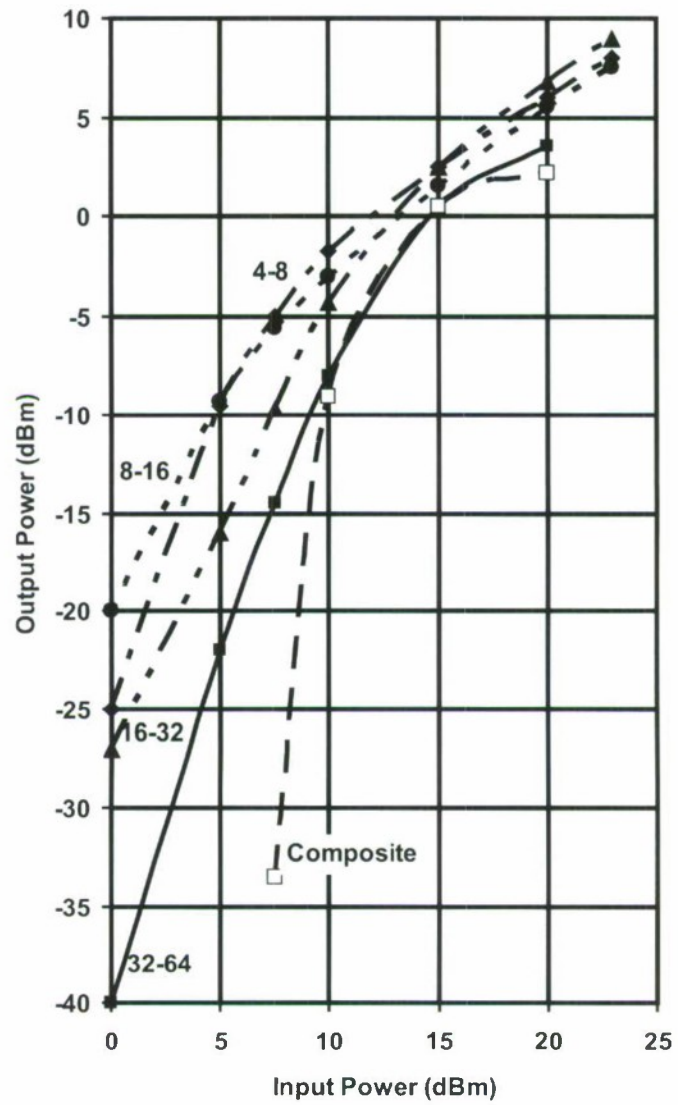


Figure 3. Power transfer curves for the four frequency doublers, identified by their input-output frequencies in GHz.

This page intentionally left blank.

### 3. CALIBRATION

#### 3.1 STATIC CALIBRATION

The rationale for the static calibration technique is that if the amplitude and phase of the quadrature drives for the SSBM can be adjusted at every point in the modulating frequency spectrum to minimize the image sideband, then it should be possible also to minimize the image sideband of each frequency component of a chirp signal by applying these same (frequency-dependent) phase and amplitude corrections to the frequency components of the chirp signal.

To determine these corrections, a computer-controlled minimization routine generates CW SSBM drive signals  $I_{DR}$  (in-phase or cosine) and  $Q_{DR}$  (quadrature or sine), having differential amplitude and phase corrections. The differential phase  $\delta\phi$  and differential amplitude  $\delta A$  corrections are applied to the SSBM drives as follows: Half of the differential phase is added to the phase of  $I_{DR}$ , and half of the differential phase is subtracted from the phase of  $Q_{DR}$ . Likewise, half of the differential amplitude is added to, and subtracted from, the amplitudes of  $I_{DR}$  and  $Q_{DR}$ , respectively. Adjustment of the differential amplitude and phase makes the cancellation of the image sideband possible. The differential corrections are controlled by a two-dimensional search routine (MATLAB® “fminsearch” function, slightly modified: The usual- and zero-term delta values were adjusted for this application, and usual-delta was added to  $y(j)$  instead of multiplying  $y(j)$ , in lines 235 through 242). This automated routine finds the corrections needed to minimize the image sideband level, as measured by a spectrum analyzer tuned to the image sideband frequency in the SSBM output. Simultaneously, a power detector connected to the P(t) port provides data for the drive amplitude  $A$  needed to normalize the WFG output level at each static calibration frequency. In this manner, a static calibration table of values of  $A$ ,  $\delta\phi$ , and  $\delta A$  is assembled for the SSBM over a modulating frequency spectrum from  $-525$  to  $+525$  MHz, in 5 MHz steps except near the ends of the frequency range, where smaller steps are used because the phase and amplitude changes are larger there. The attenuation of the AWG output reconstruction (anti-alias) filters above 525 MHz prevents accurate measurement of corrections beyond  $\pm 525$  MHz. The calibration frequencies are chosen so zero modulation frequency is not included as a calibration point to avoid errors due to SSBM carrier leakage. When the waveform generator is used to generate a CW tone the static calibration table is used, with interpolation as necessary, to determine the drive corrections during calculation of the SSBM modulating waveforms. Thus, for a CW waveform of radian frequency  $\omega$ , as a function of time  $t$ ,

$$I_{DR}(t) = (A + \delta A / 2) \cdot \cos(\omega t + \delta\phi / 2) \quad (1)$$

and

$$Q_{DR}(t) = (A - \delta A / 2) \cdot \sin(\omega t - \delta\phi / 2). \quad (2)$$

Figure 4 shows a typical SSBM drive amplitude profile  $A$  needed to obtain a uniform output level from the WFG across the  $-525$  to  $+525$  MHz SSBM modulating frequency range when generating CW tones. The general shape is due to the drive amplitude increase required by AWG output reconstruction filter attenuation as the absolute modulating frequency increases, plus the typical attenuation increase of microwave components as frequency increases.

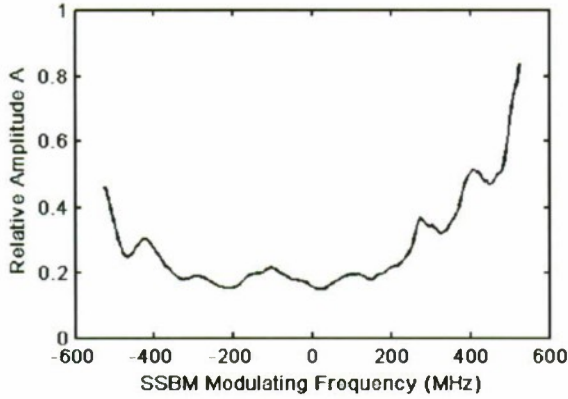


Figure 4. CW waveform drive amplitude  $A$  required for uniform WFG output levels.

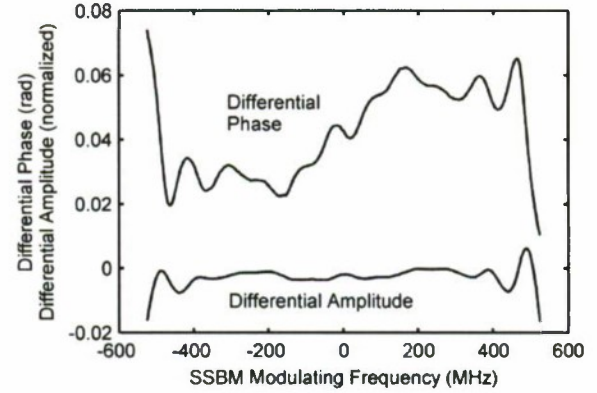


Figure 5. Differential amplitude and phase required to minimize the unwanted sideband during CW waveform generation.

Figure 5 shows typical values of  $\delta A$  and  $\delta \phi$  required to minimize the image sideband in the output of the SSBM. The differential phase has a small overall slope, which can be due to a small differential time-delay between the  $I_{DR}$  and  $Q_{DR}$  signals. Actually, the AWG used has a small hardware time-delay between its two outputs, so the cables between the AWG and the SSBM were trimmed to unequal lengths in order to reduce the slope of the differential phase to this value.

### 3.2 CHIRP WAVEFORM COMPUTATION

When the waveform generator is used to generate a chirp, the static calibration is employed during the SSBM  $I_{DR}$  and  $Q_{DR}$  waveform computation. First, the chirp waveform is computed as an ideal unity-amplitude baseband complex (analytic) time function  $e^{j\varphi(t)}$ , where  $\varphi(t)$  is the (parabolic) phase function of the baseband chirp and  $I = \sqrt{-1}$ . The time record then is shifted half a record length so the center of the chirp is at the time origin. Doing this takes the tilt out of the phase of the frequency spectrum, making it easier to visualize. The (complex) spectrum of this ideal time function is computed by discrete Fourier transform with  $4\times$  oversampling, providing access to the phase and amplitude of all the frequency components of the chirp. The oversampling is required to prevent aliasing from the tails of the chirp spectrum. Next, the spectrum is shifted half a record length to put zero frequency in the center of the spectrum record making it easier to associate with the baseband modulation frequency spectrum with its positive and negative frequencies. This spectrum is used twice. First, for the SSBM  $I_{DR}$  computation, each



of the spectral components of the chirp is multiplied by the correction  $(A+\delta A/2) \cdot e^{j \cdot \delta \phi/2}$  for frequencies between  $-525$  and  $+525$  MHz. The calibration values at  $\pm 525$  MHz are extrapolated to apply to the remainder of the spectrum out to the Nyquist frequencies ( $\pm 625$  MHz) for both positive and negative frequencies. The amplitude of the spectrum beyond the positive and negative Nyquist frequencies is set to zero. The resulting spectrum is shifted back half a record length, transformed back to the time domain, shifted half a record length,  $4\times$  down-sampled (because of the prior over-sampling), and the real part used for the SSBM  $I_{DR}$  signal. Next,  $Q_{DR}$  is computed in an analogous manner, except each of the spectral components of the chirp is multiplied by the correction  $(A-\delta A/2) \cdot e^{j \cdot (-\delta \phi/2)}$  for the same frequencies as above, and after transforming back to the time domain, the imaginary part is used.

### 3.3 DYNAMIC CALIBRATION

The CW or static correction alone is not adequate for accurate chirp generation for at least two reasons. One is the presence of nonlinear phase response in the hardware across the chirp spectrum. A second is that signal reflections in the hardware add time-delayed replicas of the signal to itself. The phase and amplitude of these reflections vary with frequency and are difficult to characterize individually. Together, these have the effect of introducing phase and amplitude errors on the chirp emerging from the frequency-doubler chain that depend on the duration and bandwidth of the chirp. An iterative approach is used here to correct these errors by analyzing the phase of the beat-note produced by the delay-line correlator to determine the chirp phase error and making appropriate compensating phase corrections during waveform computation for the next iteration. Amplitude correction during the chirp is made similarly by using the  $P(t)$  signal data (see Figure 1). Since this calibration is performed while generating the chirp signal, it is termed here a dynamic calibration. The dynamic calibration must be performed beforehand for every chirp waveform parameter set that will be needed.

This calibration also is performed by a computer-controlled optimization process. The  $P(t)$  and beat-note signals are captured by a digital storage oscilloscope and processed to determine the deviations from ideal. The amplitude error is determined directly from the power measurement. The amplitude is given by the square-root of the power detector signal, and compared to a reference value to determine the amplitude error throughout the chirp. The phase error is derived from the deviation of the phase of the beat-note signal from the desired value. The beat-note results from the square-law detection of the chirp summed with a delayed version of itself, so the beat-note phase is the phase of the chirp minus the phase of the delayed chirp, where the delay is the propagation time difference in the two arms of the delay-line correlator in Figure 1. Thus the correlator output power detector signal is

$$A_c^2(t) + A_c^2(t - \delta t) + 2 \cdot A_c(t) \cdot A_c(t - \delta t) \cdot \cos(\phi_c(t) - \phi_c(t - \delta t)), \quad (3)$$



where  $A_c(t)$  and  $\varphi_c(t)$  are the output chirp amplitude and phase, respectively, and  $\delta t$  is the differential delay of the correlator. The first two terms result from the chirp power fluctuations and have spectral energy at DC and low frequencies. The last term is the cross-product term containing the desired phase information. Now, the chirp phase is the sum of the quadratic ideal-chirp phase plus a phase error  $\varphi_e(t)$ . Since the phase difference between an ideal chirp and its delayed replica is a linear phase function corresponding to the beat frequency  $f_b = BW \cdot \delta t / T$ , where  $T$  and  $BW$  are the chirp period and bandwidth respectively, one can obtain the difference of the chirp phase errors  $\varphi_e(t) - \varphi_e(t - \delta t)$  by filtering out the first two terms in the detector signal expression above and phase-demodulating the last term in software with a carrier frequency of  $f_b$ . If the delay is short enough, this phase difference divided by  $\delta t$  is equal to the time derivative of the chirp phase error:

$$\lim_{\delta t \rightarrow 0} \left( \frac{\varphi_e(t) - \varphi_e(t - \delta t)}{\delta t} \right) = \frac{\partial \varphi_e(t)}{\partial t}. \quad (4)$$

Thus, by dividing the residual (i.e., demodulated) beat-note phase by  $\delta t$  and integrating over time, the chirp phase error can be estimated.

For the result to be accurate, the value of  $\delta t$  must be known accurately. In the present work, the delay is about 8 ns, which is about 1.7 % of the chirp period of interest, 512 ns. It is necessary to know the delay to about 2.5 parts in  $10^3$  if the cumulative linear phase error is to be less than a radian in this case. The actual delay was determined by manually frequency-sweeping the correlator assembly and measuring the null frequencies across the 2 to 18 GHz band. These frequencies were plotted, and the best linear fit used to determine the slope, which is the reciprocal of the time delay. Figure 6 shows the residuals of the measured null frequencies after the linear fit. The residual null frequency errors generally are less than  $\pm 1$  MHz across the band. This result was obtained using identical matched-line power dividers [10] in the correlator, with the divider ports swapped on the ends of the lines to cancel systematic phase differences that might exist at the divider ports. A length of coaxial cable was used for the time delay.

These residuals affect the accuracy of the chirp phase error reconstruction obtained from the beat-note phase as described above. Since the correlator nulls are spaced about 125 MHz apart, a residual of 1 MHz corresponds to about  $2\pi/125$  radians phase departure from linear phase, or about 50 mrad phase angle.

To determine the effect of these residuals on the phase correction accuracy for a chirp of a certain bandwidth and period, the residual is multiplied by  $2\pi$  and integrated over the period of the chirp for the appropriate bandwidth, since the phase error due to the residuals can be calculated just as the chirp phase

error was calculated from the beat-note phase error above. This has been done for a 2–18 GHz, 512 ns chirp and the result is plotted in Figure 7. The magnitude of this phase error scales as the chirp duration (for a fixed correlator delay) and with the correlator error over the chirp bandwidth. The present application required good chirp phase accuracy because large target delays had to be accommodated with respect to the receiver's demodulation chirp timing. In principle, it may be possible to use the correlator frequency-null data to correct the phase measurement of the chirp beat-note during calibration but that has not been attempted in the present work. Note that for many other applications, the receiver's demodulation chirp can be aligned accurately with the received chirp and larger chirp phase errors may be tolerated.

Ten records of the correlator and power signals are averaged for each iteration of the dynamic calibration routine. Signal processing requires discarding power and correlator signal data at each end of the data records for a duration equal to half the correlator delay and splicing-in the average of the same number of adjacent samples. The modified correlator signal record is demodulated, Hamming-weighted, and the result zero-padded with the weighted signal length and transformed to obtain the correlator signal spectrum. For each iteration of the routine only fractions of the measured amplitude and phase errors are applied as corrections when calculating the corrected waveform. Because the amplitude and phase errors

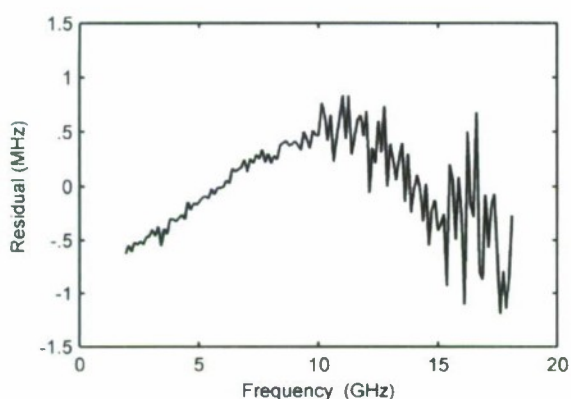


Figure 6. Residuals after the best linear fit to correlator null frequency values over the frequency range 2–18 GHz.

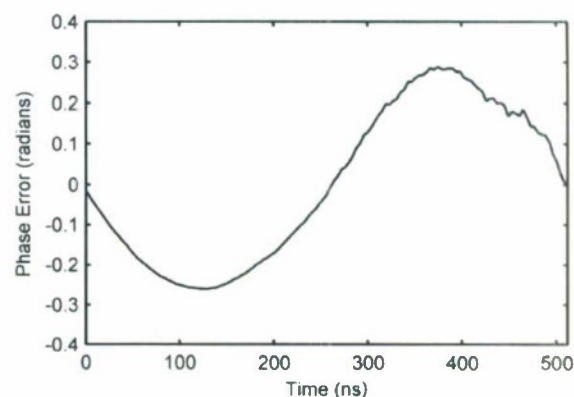


Figure 7. Predicted phase error of a 2–18 GHz, 512 ns chirp due to correlator errors.

are coupled it is necessary to have one of the errors corrected more slowly than the other to avoid instability during convergence. Accurate timing of the power and beat-note signal capture is required to be sure the correction is applied at the proper time in the chirp waveform. In practice, it sometimes is found desirable to average amplitude and phase corrections over several sample points to minimize noise and ensure stability. With these simple precautions it is possible to perform a dynamic calibration with several tens of iterations.

This page intentionally left blank.

## 4. CARRIER LEAKAGE SUPPRESSION

### 4.1 EXPOSING THE CARRIER LEAKAGE

When computing a chirp waveform to drive the SSBM, the chirp is mathematically described as starting at frequency  $-BW/2$  and ending at  $+BW/2$ , where  $BW$  is the total chirp bandwidth. The phase function for this chirp is

$$\varphi_c(t) = \pi \cdot BW \cdot \left( -t + t^2 / T \right). \quad (5)$$

This function is zero at  $t = 0$  and  $t = T$ , i.e., there is no phase tilt, or equivalently, frequency offset, in this waveform. If generated repetitively, the starting and ending values of the SSBM drives are similar except for changes due to the calibrations discussed above. If repeated, the resulting chirp train will produce a comb in the frequency domain, and there will be a spectral line at zero frequency (the SSBM carrier frequency) that will mask the actual SSBM carrier leakage.

To expose the carrier leakage during repetitive chirp operation so it can be measured and nulled, it is necessary to shift the frequency comb of the repetitive chirp train. A shift of half the comb frequency spacing can be obtained by adding a phase ramp (tilt) of  $\pi$  radians across the chirp phase function. However, the tilt must appear to be a continuous function across the repetitive chirp train, and this can be done by adding to the next chirp's phase with a step (bias) of  $\pi$  radians as well as the tilt of  $\pi$  radians. At the end of the second chirp,  $I_{DR}$  and  $Q_{DR}$  have the same values they had at the beginning of the chirp pair ( $2\pi$  radians is indistinguishable from 0 radians), so the pair can be repeated, creating a virtual continuation of the phase tilt indefinitely. Waveforms computed from two such chirp phase functions and concatenated in this manner are called "dual chirp" waveforms here. The chirp frequency offset resulting from the phase ramp can be compensated for by changing the LO frequency of the multiplier chain output down-converter, if necessary.

If the chirp band is not symmetrical about zero modulating frequency, an algorithm is used to slightly readjust the ending frequency as needed so the ending phase of the chirp is a multiple of  $2\pi$ .

### 4.2 CARRIER NULL SERVO

While temperature control of the SSBM and the laboratory provides enough stability that the carrier null can be held below  $-55$  dBe with only occasional manual adjustment, long-term stability can be enhanced through the use of the two-channel carrier null servo (see Figure 1). Basically, the I and Q components of the carrier leakage are demodulated separately and used to control the DC inputs to the



bias tees to null the leakage. The narrow-band carrier filter limits the total power to the carrier leakage demodulator input. The phasing of the demodulated carrier leakage I & Q signals with respect to the SSBM I & Q drives can be adjusted by changing the length of the LO drive cable.

The servo circuit consists of an analog portion followed by a digital portion. The analog portion contains a low-pass signal filter, amplification, and an analog absolute-value circuit. The absolute values of the demodulated I and Q leakage signals are used to drive voltage-to-frequency converters, which produce square-wave output frequencies proportional to the quadrature leakage component magnitudes. The polarity of the error is obtained from the absolute value circuit. The square waves and polarity signals drive digital counters up or down at a rate proportional to the error voltage, in effect being a digital loop integrator. The counts are sent to D/A converters, whose outputs are sent to the appropriate bias tees, thus closing the loops. Counters were chosen as the integrating elements so the loops could be opened by removing the counter drives, holding the integrator values indefinitely. During closed-loop operation the servo holds the carrier leakage below  $-65$  dBc under ordinary laboratory conditions.

Since DC and low-frequency voltages on the SSBM I & Q drives affect the carrier null, it is important to avoid power-line frequency currents in these drives. This requires sturdy ground connections between the AWG module and the SSBM and the use of drivers having output isolation for the bias-tee drives.



## 5. PERFORMANCE

### 5.1 SSBM OUTPUT SPECTRA

Figure 8 shows superimposed SSBM output spectra for CW outputs at four modulation frequencies using the corrections obtained with a static calibration. The output levels at the different frequencies are slightly different because the static calibration normalized the output from the doubler chain, while the data are taken from a sample of the drive for the first doubler. The image sidebands and spurs as well as the carrier leakage generally are below the  $-65$  dBc level.

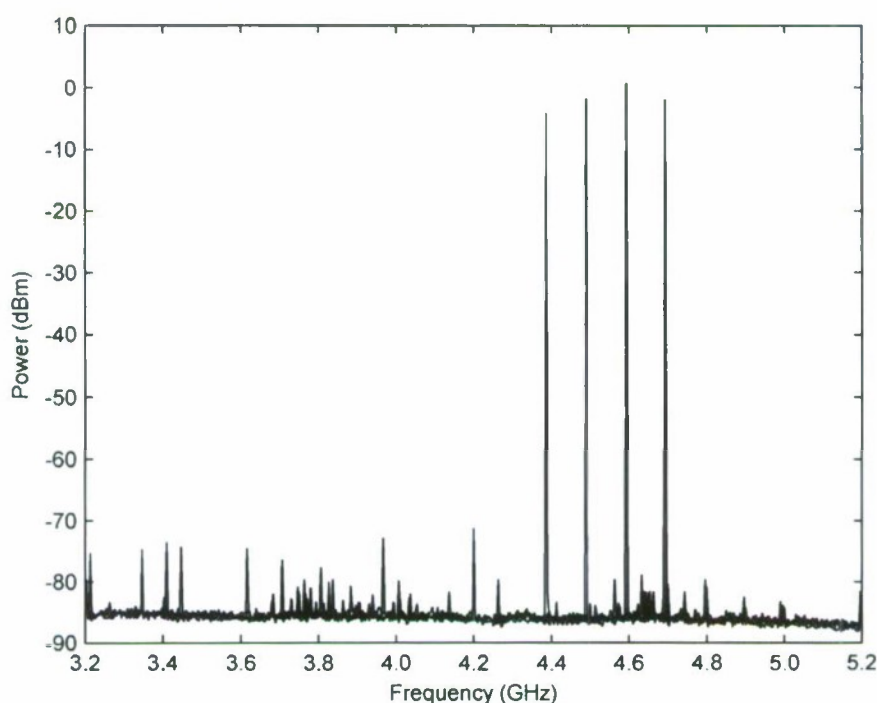
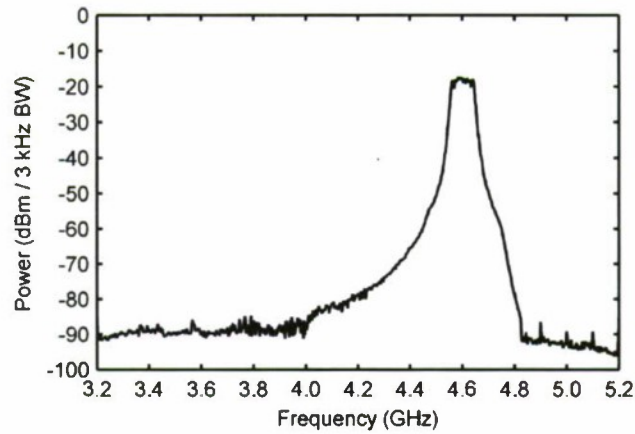


Figure 8. Superimposed SSBM CW output spectra, using static correction only. The modulating frequencies are 188, 292, 396, and 495 MHz.

It is of interest to know if the SSBM image sideband suppression obtained with the CW calibration is effective when chirp waveforms are playing. One way to visualize the image suppression is to generate

a narrow-band chirp near one edge of the modulation band and look for its image near the other edge of the band. Figure 9 shows the SSBM output spectrum of a +350 to +450 MHz, 512 ns period repetitive chirp train signal, and it can be seen the image level is approximately -65 dBc.

In Figure 10, the chirp period has been decreased to the minimum, 102.4 ns, and the image level is about the same. Note however, the appearance of a spur band just below the Nyquist frequency of 4.2 GHz minus 0.625 GHz, or 3.575 GHz. This spur appears as the spectral energy of the SSBM modulation above 500 MHz rises but it disappears if the signal spectrum is truncated at 525 MHz during waveform computation.



*Figure 9. SSBM output spectrum of a +350 to +450 MHz, 512 ns period repetitive chirp train.*

Finally, Figure 11 shows the SSBM output spectrum for a +250 to +450 MHz, 102.4 ns chirp train, chosen because the chirp rate (MHz/ns) is comparable to the chirp rate of a full-band, 512 ns period chirp. Here it appears the image level may only be 55 dB down, although the broadened spectrum makes true evaluation of the image level difficult.

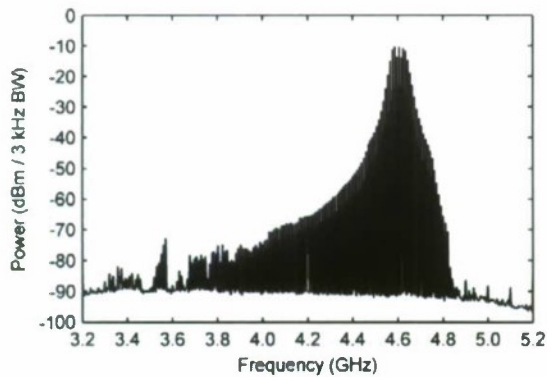


Figure 10. SSBM output spectrum of a +350 to +450 MHz, 102.4 ns period repetitive chirp train.

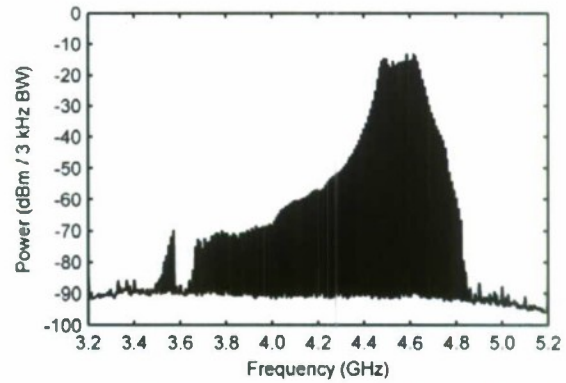


Figure 11. SSBM output spectrum of a +250 to +450 MHz, 102.4 ns period repetitive chirp train.

## 5.2 CHIRP STOP-START TRANSIENTS

For applications requiring a train of contiguous chirps, the transient duration at the end of one chirp and the beginning of the next can be of concern. Factors which influence the transition from one chirp to the next include the response of the AWG and the SSBM, reflections in the signal train, and the method for computing the SSBM drive waveforms. For the present chirp waveform, these transients were characterized by demodulating the WFG output waveform using a CW LO frequency equal to the starting or ending frequency of the chirp and observing the beat note. Figure 12 shows a typical result for a repetitive 12.5 GHz, 512 ns chirp, extracted from an oversized chirp used for dynamic calibration. AWG reconstruction filter phase compensation was applied during SSBM drive waveform computation.

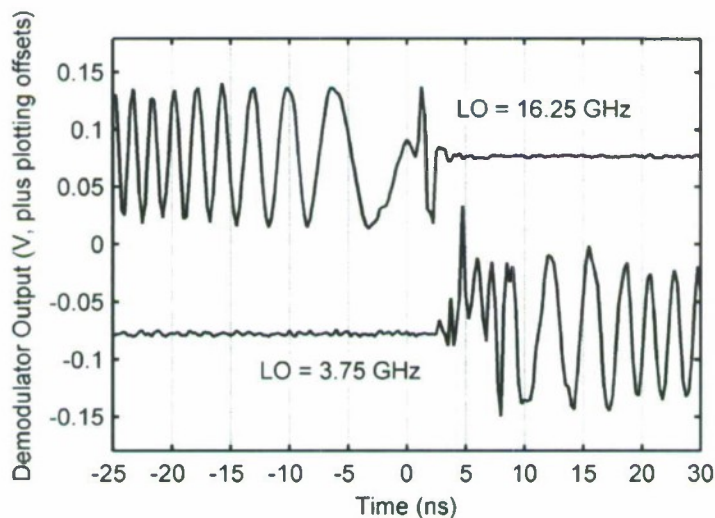


Figure 12. Stop (top trace) and start (lower trace) WFG output transients.

The principal factors contributing to the transient duration in the present WFG implementation seem to be the response of the AWG reconstruction filter and the method of waveform computation. While the waveform computation algorithm forces the beginning and ending phase of the chirp to be zero or a multiple of  $2\pi$ , the quadrature SSBM drive has a discontinuity in the first time derivative of its phase at the interface of contiguous chirps. The minimum transient duration one can expect can be viewed by loading the AWG with a repetitive train of two contiguous CW waveform segments: One at the anticipated chirp start frequency and one at the anticipated chirp stop frequency. The AWG I and Q outputs for the extreme case of switching from a +500 MHz CW waveform to a -500 MHz CW waveform are shown in Figure 13. The phase of both waveforms at zero time is zero. It is believed the large Q-channel transient, (and to a lesser extent the I-channel transient), causes the momentary

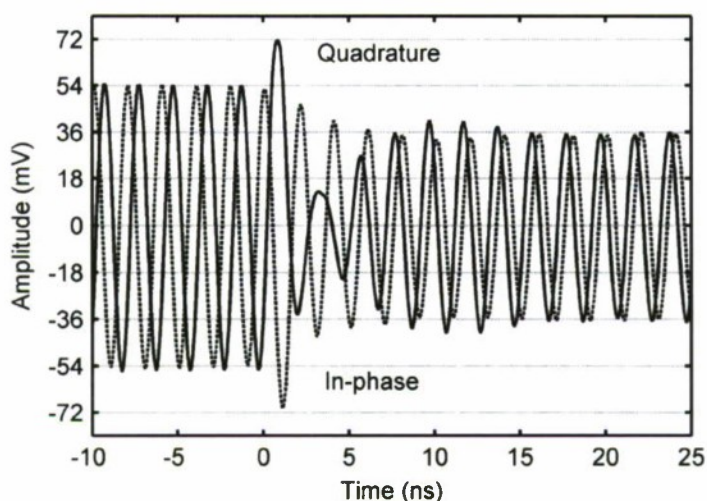


Figure 13. AWG I & Q outputs for a +500 MHz to -500 MHz CW waveform transition, measured with a 4 GSa/s, 1 GHz BW digital storage oscilloscope, and resampled at  $2.5\times$  for plotting.

appearance of the image sideband in addition to direct phase errors in the SSBM output. Changing the beginning and ending phases of chirps from zero to other values did not substantially change the duration of the transient observed using contiguous chirp waveforms.

The spectrum correction applied during SSBM chirp drive waveform computation also contributes to the end transients. The multiplication of the chirp spectrum by the amplitude and phase corrections in the frequency domain is equivalent to a convolution by the transform of those corrections in the time domain. Thus, it is apparent that the convolution will introduce distortions at the ends of the chirp. In the present implementation, the amplitude correction across the spectrum produces the largest increase in the transient, while the differential amplitude and phase corrections used to suppress the image signal in the



SSBM output contribute relatively little to the transient. Thus in the hardware it is important to obtain the flattest response possible across the chirp spectrum before correction.

One technique to minimize the effect of spectral compensation on the end transients is to compute the SSBM drive for an oversized chirp during dynamic calibration, i.e., one that is oversized in both bandwidth and duration by the same factor, and to then extract a central portion of the desired size for use, as has been done for the data in Figure 12. This has been used successfully to minimize the end transients, although it is applicable only for chirp bandwidths smaller than the maximum bandwidth capability of the hardware. For large bandwidths, it also is advantageous to add compensation for the AWG reconstruction filter phase shift while computing the waveform during dynamic calibration.

### 5.3 TIME-SIDELobe LEVELS

Figures 14 and 15 show the phase and amplitude errors and the correlator signal spectrum measured after dynamic calibration of a 15.625 GHz, 640 ns dual chirp waveform at the output of the WFG. Two

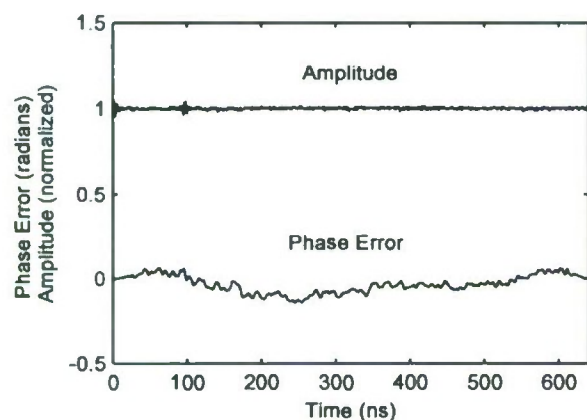


Figure 14. Measured chirp amplitude and phase error of a 15.625 GHz, 640 ns dual chirp waveform after dynamic calibration.

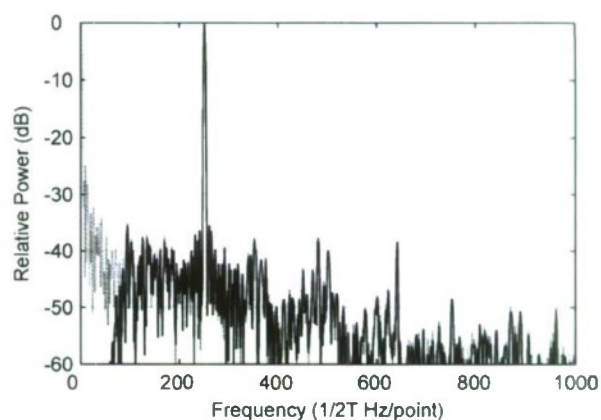


Figure 15. Filtered and unfiltered correlator spectra of a 15.625 GHz, 640 ns dual chirp waveform after dynamic calibration.

spectra are shown in Figure 15, one without and one with a high-pass frequency filter to eliminate the baseband spectrum due to power fluctuations in the correlator signal. The correlator delay was 8 ns. Typically, a sidelobe level approaching -40 dB is achieved in the correlator signal spectrum during a calibration relative to this (imperfect) correlator for chirp lengths of 512 ns and greater.

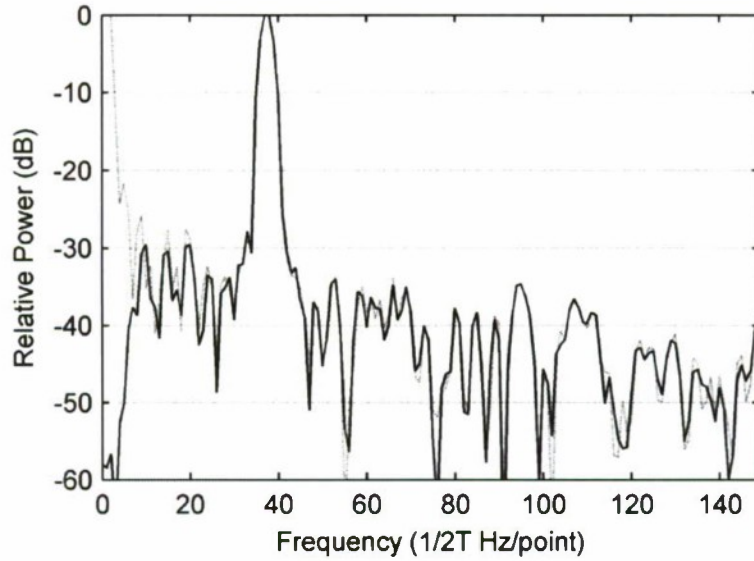


Figure 16. Correlator spectrum of a 12.5 GHz, 128 ns dual chirp after dynamic calibration.

Figure 16 shows the sidelobes of a 12.5 GHz, 128 ns chirp after dynamic calibration. The correlator delay was 1.5 ns. As might be expected, the sidelobe level rises at very short chirp lengths. Before dynamic calibration, the sidelobes were  $-10$  dBc.

#### 5.4 CHIRP SPECTRA AT THE WFG OUTPUT

Figure 17 shows the spectrum of a narrowband chirp at the output of the down-converter. At 3 GHz and some other nearby frequencies are a number of fixed frequency spurs which come from the down-converter LO. They originate in the 14.3 GHz frequency source, where they are  $-75$  dBc. In the doubler chain output, they are  $<55$  dB below the output signal level. (There is a spur just below 2 GHz, which is a down-converter mixing product more fully described below.)

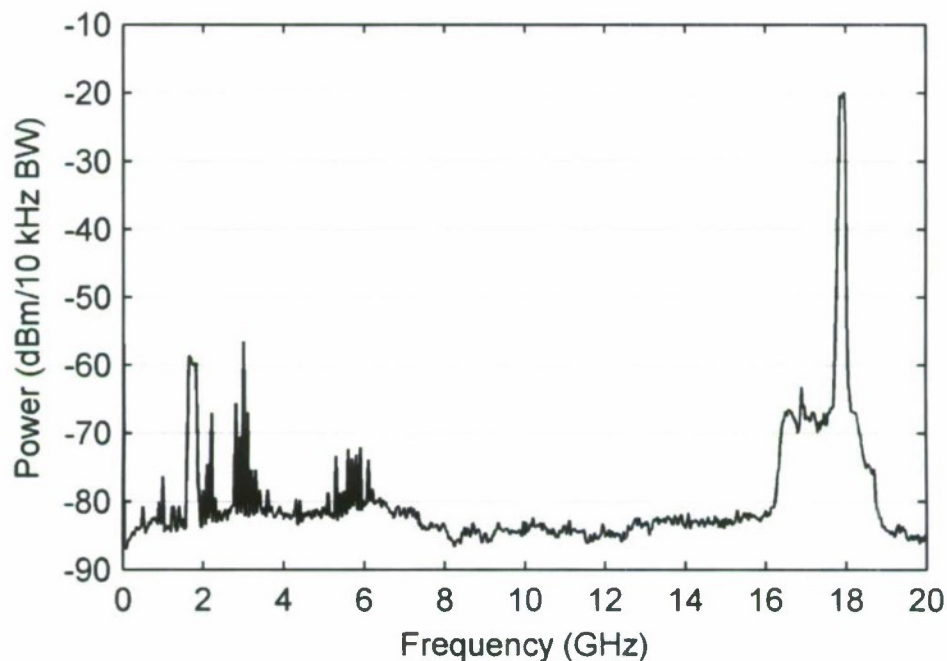


Figure 17. Spurious frequencies in the WFG output, while generating narrow band (0.16 GHz), 512 ns chirps centered at 17.92 GHz.

There are two spurs originating in the down-converter and they are shown in Figure 18. Here are plotted the spectra of 0.8 GHz, 512 ns chirps programmed for different center frequencies across the WFG output bandwidth. The chirp bands are contiguous and the spectra obtained while each of them was playing are plotted with 20 dB vertical displacements so the presence of any spurs could be seen. There are two spurs: One moves up in frequency as the chirp band moves up (top-half of Figure 18), and the other moves down as the chirp band continues to move up (lower-half of Figure 18). The absolute level of the top trace only is correct, and the resolution bandwidth is 10 kHz. (The output level of the WFG is -1.5 dBm.) The rising-frequency spur is the down-converter intermodulation product  $2RF \times 2LO$ . The falling-frequency spur is the product of the third harmonic of the signal after the third doubling (Ka-band) and 2LO. The latter is surprising because there is a low-pass filter on the down-converter input to reject the third harmonic of the fourth doubler. That filter was measured by the manufacturer at 90 GHz and found to have 40 dB attenuation, and they state the design should attenuate at that level well beyond 2LO (114.4 GHz), but that it had never been measured there. However, the spurs are approximately -40 dBc or less across the operating bandwidth of the down-converter output and are acceptable for the present application.

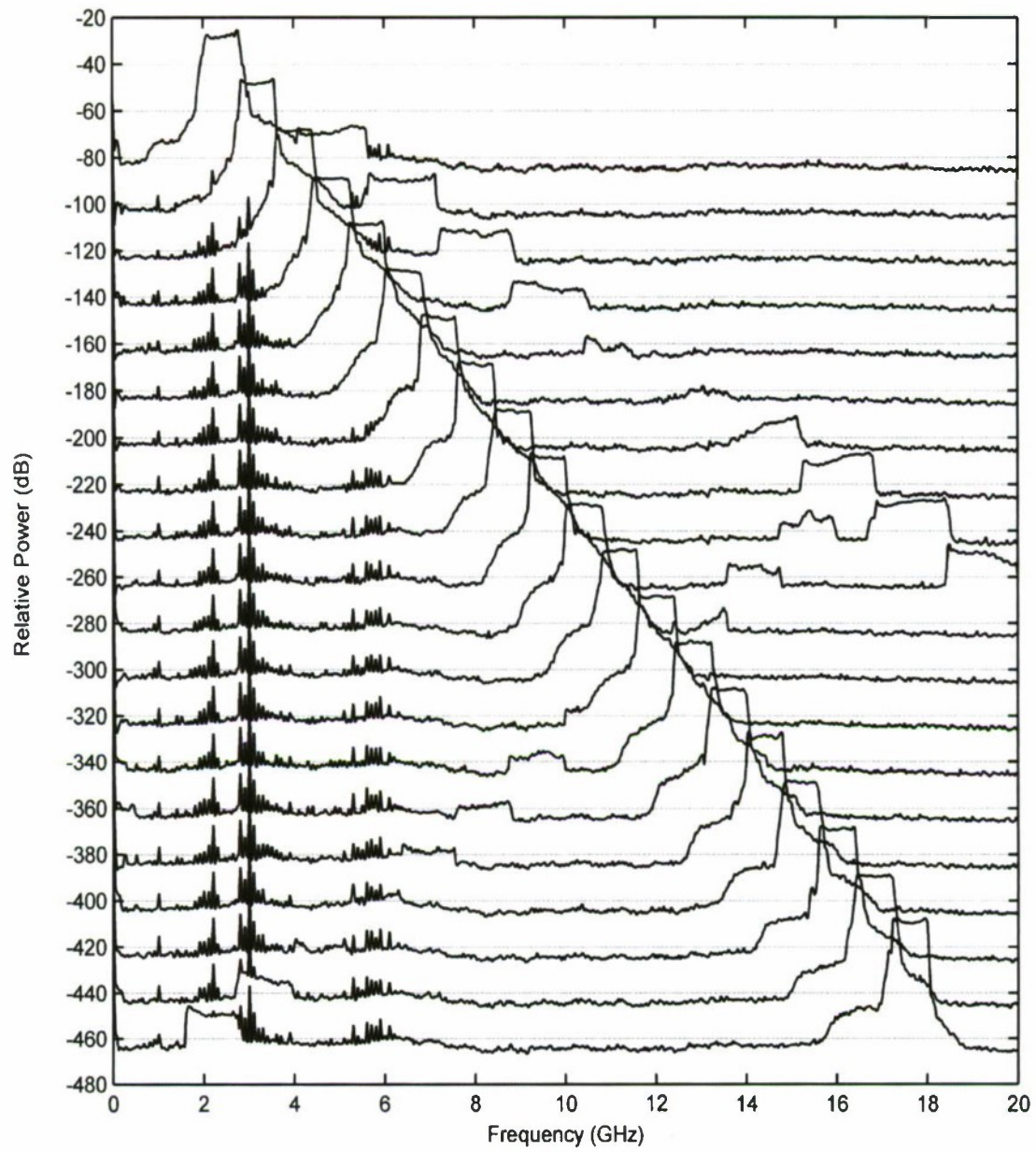


Figure 18. Down-converter spurs for 0.8 GHz, 512 ns dual up-chirps placed across the 2–18 GHz spectrum. The ordinate of the top trace only is dBm/10kHz BW, and the remaining spectra have been displaced vertically for clarity.



Figure 19 shows WFG output spectra for 12.5 GHz BW chirps having three different chirp periods. The chirps were computed without oversizing, so the effect of the starting transient is somewhat larger than for chirps computed with oversizing. There was no dynamic calibration for these data so that the effect of reflections in the hardware train, which increase the power fluctuations across the band as the chirp length diminishes, could be shown. The response flatness at the 8192 ns chirp duration is due principally to the spectrum analyzer calibration and its differences from the response of the power detector used for the CW calibration. On the low end of the 8192 ns chirp-length data, the CW spurs reported above are seen.

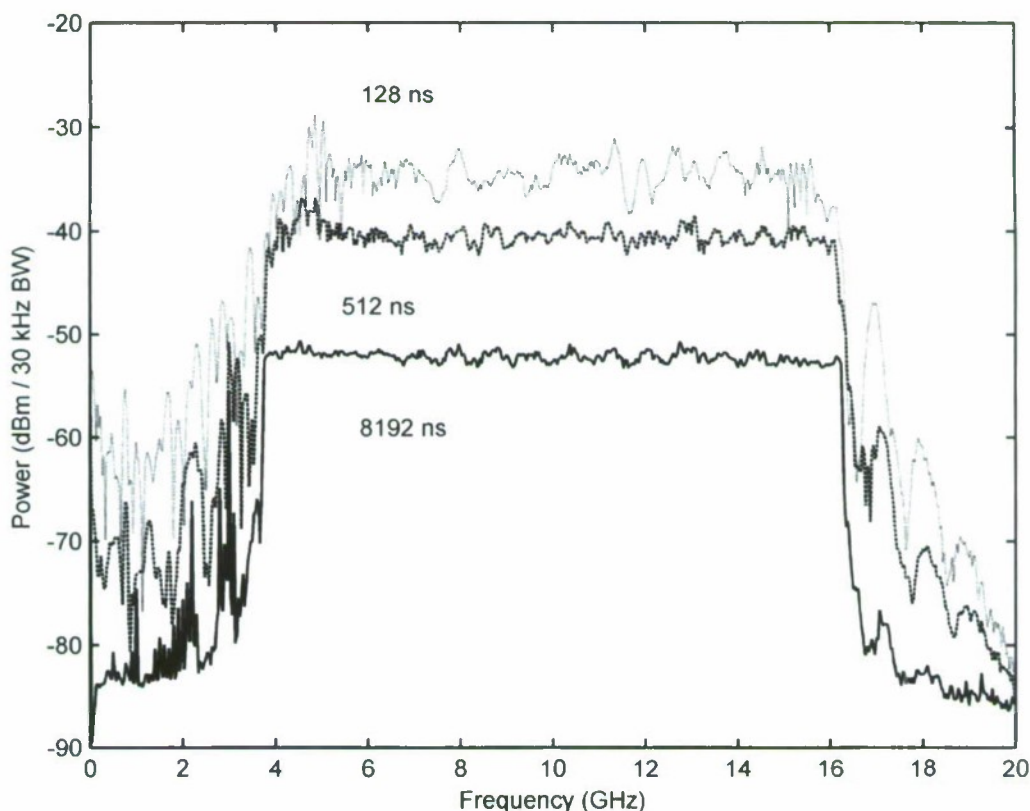


Figure 19. WFG output spectra of 12.5 GHz chirps for three different chirp durations.

At 128 ns chirp length, it has been observed that dynamic calibration reduces the power fluctuations slightly, but does not eliminate them. The out-of-band spurs that appear as the chirp length decreases are presumed to be due to amplitude and phase modulations arising in the hardware chain and they do not decrease appreciably after dynamic calibration either. Presumably, a hardware chain with smaller amplitude and phase errors across the band would provide smoother in-band response and lower out-of-band spurs.

This page intentionally left blank.

## 6. SUMMARY

A WFG design optimized for very short, very wideband linear-FM microwave chirp generation has been presented together with measurements of its performance. The waveform computation and static calibration procedures presented here demonstrate that SSBM carrier leakage and image sideband levels can be reduced to insignificant values when generating chirp waveforms, thereby eliminating the need for one frequency doubler in the typical chirp generator architecture. The dynamic calibration technique produces substantial improvement in the time sidelobes of the chirp waveform. A sidelobe level approaching  $-40$  dBc for 12.5 GHz, 512 ns chirps has been demonstrated using a time-delay correlator as the reference, and presumably the same sidelobe level could be reached during calibration of a system employing the WFG. An error source for applications that requires contiguous chirps from a single WFG can be the stop-start transients, which create a gap in the useable waveform at the chirp ends. The stop-start transients diminish somewhat for smaller bandwidths, and in general the performance of the WFG improves with smaller bandwidths and longer chirp lengths, as might be expected. The transient duration is a function of the AWG and SSBM bandwidths, and these must be considered in the WFG design if the transient duration is of importance in the planned application.

This page intentionally left blank.



## REFERENCES

1. M.I. Skolnik, *Radar Handbook*, New York: McGraw-Hill, 2008, Chapter 8.
2. W.J. Caputi, "Stabilized linear FM generator," *IEEE Trans. On Aerospace and Electronic Systems*, vol. AES-9, no. 5, pp. 670–678, Sept. 1973.
3. M.Z. Straayer, A.V. Messier, and W.G. Lyons, "Ultra-linear superwideband chirp generator using digital compensation," *IEEE MTT-S Int. Microwave Symp. Dig.*, 11–16 June 2006, pp. 403–406.
4. L.O. Eber and H.H. Soule, Jr., "Digital generation of wideband LFM waveforms," *Proc. 1975 IEEE International Radar Conference*, pp. 170–5.
5. T. Kawanishi, T. Sakamoto, and M. Izutsu, "Ultra-wideband frequency chirp signal generation by using high-speed optical frequency control with optical single-sideband modulation technique," *Microwave Photonics, 2006. MWP '06. International Topical Meeting on*, Grenoble, Oct. 2006, pp. 1–4.
6. G.G. Brown, B.C. Dian, K.O. Douglass, S.M. Geyer, S.T. Shipman, and B.H. Pate, "A broadband Fourier transform microwave spectrometer based on chirped pulse excitation," *Rev. Sci. Instr.*, vol. 79, no.5, 053103, pp. 1–13, May 2008.
7. W.D. Gallaway, K.F. Luckschciter, E.H. Cowen, and J.W. Wilhelm, "A direct digitally synthesized exciter achieving near theoretical performance for an operational SAR system," *Proc. 1988 IEEE National Radar Conference*, 20–21 Apr. 1988, pp. 22–27.
8. S.-Y. Kim and N.-H. Myung, "Wideband linear frequency modulated waveform compensation using system predistortion and phase coefficients extraction method," *IEEE Microwave and Wireless Components Letters*, vol. 17, no. 11, pp. 808–810, Nov. 2007.
9. The Mathworks, Inc. ([www.mathworks.com](http://www.mathworks.com)).
10. T.J. Russell, "Matched-Line Directional Dividers," *IEEE Trans. Microwave Theory and Techniques*, vol. MTT-41, no. 6, pp. 1094–1104, June/July 1993.

This page intentionally left blank.

REPORT DOCUMENTATION PAGE				Form Approved OMB No. 0704-0188	
Public reporting burden for this collection of information is estimated to average 1 hour per response, including the time for reviewing instructions, searching existing data sources, gathering and maintaining the data needed, and completing and reviewing this collection of information. Send comments regarding this burden estimate or any other aspect of this collection of information, including suggestions for reducing this burden to Department of Defense, Washington Headquarters Services, Directorate for Information Operations and Reports (0704-0188), 1215 Jefferson Davis Highway, Suite 1204, Arlington, VA 22202-4302. Respondents should be aware that notwithstanding any other provision of law, no person shall be subject to any penalty for failing to comply with a collection of information if it does not display a currently valid OMB control number. <b>PLEASE DO NOT RETURN YOUR FORM TO THE ABOVE ADDRESS.</b>					
1. REPORT DATE (DD-MM-YYYY) 29 December 2010		2. REPORT TYPE Technical Report		3. DATES COVERED (From - To)	
4. TITLE AND SUBTITLE  Digital Wideband Linear-FM Chirp Waveform Generator				5a. CONTRACT NUMBER FA8721-05-C-0002	
				5b. GRANT NUMBER	
				5c. PROGRAM ELEMENT NUMBER	
6. AUTHOR(S)  David G. Kocher, Group 106				5d. PROJECT NUMBER 1963	
				5e. TASK NUMBER 11	
				5f. WORK UNIT NUMBER	
7. PERFORMING ORGANIZATION NAME(S) AND ADDRESS(ES)  MIT Lincoln Laboratory 244 Wood Street Lexington, MA 02420-9108				8. PERFORMING ORGANIZATION REPORT NUMBER  TR-1157	
9. SPONSORING / MONITORING AGENCY NAME(S) AND ADDRESS(ES) RRTO/DDR&E 241 18 <sup>th</sup> Street Suite 200B Arlington, VA 22202				10. SPONSOR/MONITOR'S ACRONYM(S)	
				11. SPONSOR/MONITOR'S REPORT NUMBER(S) ESC-TR-2010-077	
12. DISTRIBUTION / AVAILABILITY STATEMENT  Approved for public release; distribution is unlimited.					
13. SUPPLEMENTARY NOTES					
14. ABSTRACT  The design and performance of a digital linear-FM chirp waveform microwave generator having a maximum bandwidth capability of 16 GHz and minimum chirp duration of 102.4 ns are described along with techniques developed for the compensation of hardware errors. Emphasis is on optimization and characterization of chirp quality while operating with large bandwidths and chirp durations less than a microsecond.					
15. SUBJECT TERMS					
16. SECURITY CLASSIFICATION OF:			17. LIMITATION OF ABSTRACT  Unclassified	18. NUMBER OF PAGES  41	19a. NAME OF RESPONSIBLE PERSON
a. REPORT Unclassified	b. ABSTRACT Unclassified	c. THIS PAGE Unclassified			19b. TELEPHONE NUMBER (include area code)

This page intentionally left blank.